Supplementary Figures

Figure S1

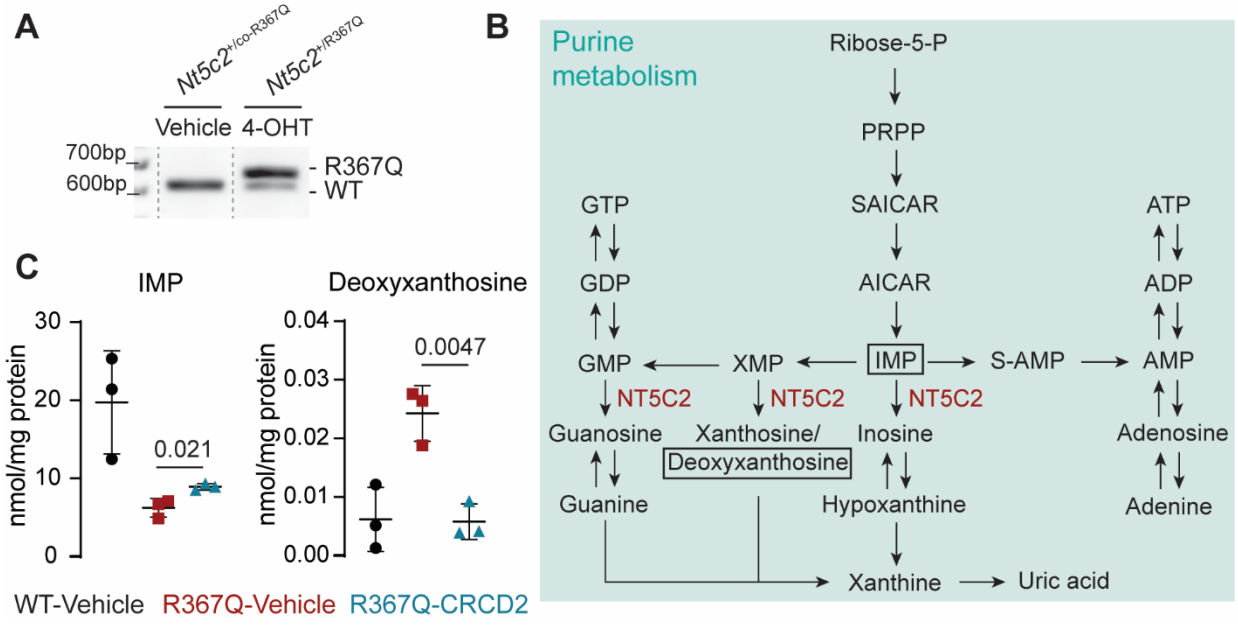

Figure S1. CRCD2 metabolic effect in NT5C2 R367Q mutant ALL mouse cells. (**A**) PCR amplification of Nt5c2 wild-type and R367Q mutant alleles after 4-OHT treatment. (B) Diagram of the purine de novo biosynthesis and salvage pathway. (C) Levels of IMP and deoxyxanthosine per mg of protein, detected in NT5C2 wild-type or R367Q mouse ALL lymphoblasts treated with vehicle or CRCD2.Graph shows mean ± SD of three replicates per sample. P values were calculated using two-sided Student's t-test.

Figure S2

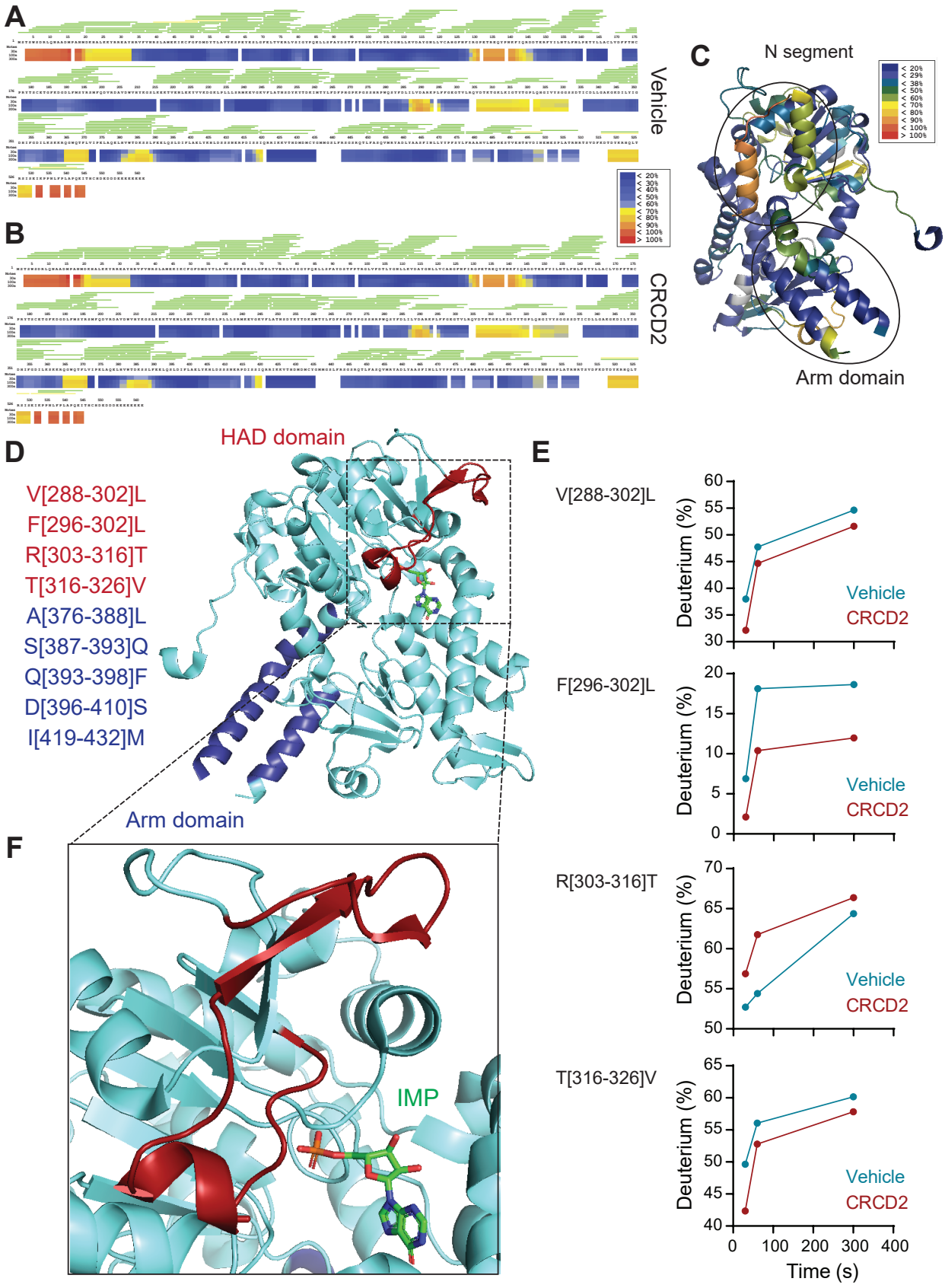
A
Vehicle
B
CRCD2
C
N segment
Arm domain
D
HAD domain
V[288-302]L
F[296-302]L
R[303-316]T
T[316-326]V
A[376-388]L
S[387-393]Q
Q[393-398]F
D[396-410]S
I[419-432]M
Arm domain
E
V[288-302]L
F[296-302]L
R[303-316]T
T[316-326]V
Deuterium (%)
Vehicle
CRCD2
Time (s)
F
IMP

Figure S2. Hydrogen-Deuterium Exchange Mass Spectrometry analysis of NT5C2 R367Q and CRCD2. (**A**) Heatmap showing Deuterium exchange percentage at 30, 100 and 300 seconds of reaction in the different regions of NT5C2 in the presence of IMP. Analyzed peptides are shown in green. (**B**) Heatmap showing Deuterium exchange percentage at 30, 100 and 300 seconds of reaction in the different regions of NT5C2 in the presence of IMP and CRCD2. Analyzed peptides are shown in green. (**C**) Crystal structure of NT5C2 R367Q (PDB id: 6DDH) showing HDX rates at 30 secs. The highly dynamic regions of the N segment and arm domain are highlighted. (**D**) Crystal structure of NT5C2 R367Q (PDB id: 6DDH) showing peptides with different pattern of Deuterium exchange in the presence of CRCD2. Arm domain peptides are shown in blue and peptides belonging to the HAD III region appear in red. (**E**) Deuterium exchange percentage at 30, 100 and 300 sec of 4 HAD domain peptides in the presence and in the absence of CRCD2. (**F**) Close-up view of the crystal structure of NT5C2 R367Q (PDB id: 6DDH) showing the proximity of the differential peptides of the HAD III domain and the binding region of the substrate.

Figure S3

A

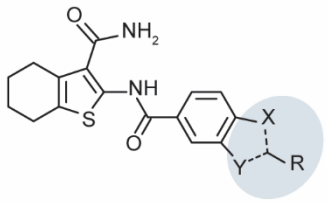

CMPD	X	Y	R	Activity
CRCD2	NH	N	H	Active
CRCD47	NH	N	CH_3	Active
CRCD48	NCH_3	N	H	Active
CRCD18	N	S	H	Inactive
CRCD74	CH	NCH_3	H	Inactive

B

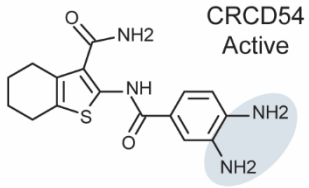

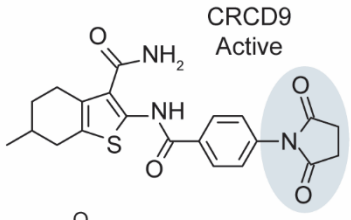

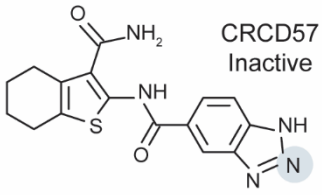

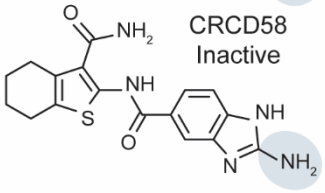

C

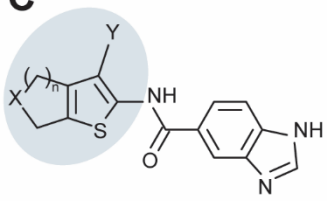

CMPD	n	X	Y	Activity
CRCD2	2	CH_2	$CONH_2$	Active
CRCD49	3	CH_2	$CONH_2$	Inactive
CRCD39	2	$CHCH_3$	$CONH_2$	Inactive
CRCD41	1	CH_2	$CONH_2$	Active
CRCD42	2	O	$CONH_2$	Inactive
CRCD40	2	CH_2	$CONHCH_3$	Inactive
CRCD43	2	CH_2	$COOCH_3$	Inactive
CRCD22	2	CH_2	CN	Active
CRCD76	2	CH_2	CO_2H	Inactive

D

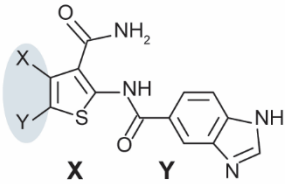

CMPD	X	Y
CRCD50	H	H
CRCD51	H	CH_3
CRCD52	CH_3	CH_3
CRCD53	CH_3	H

E

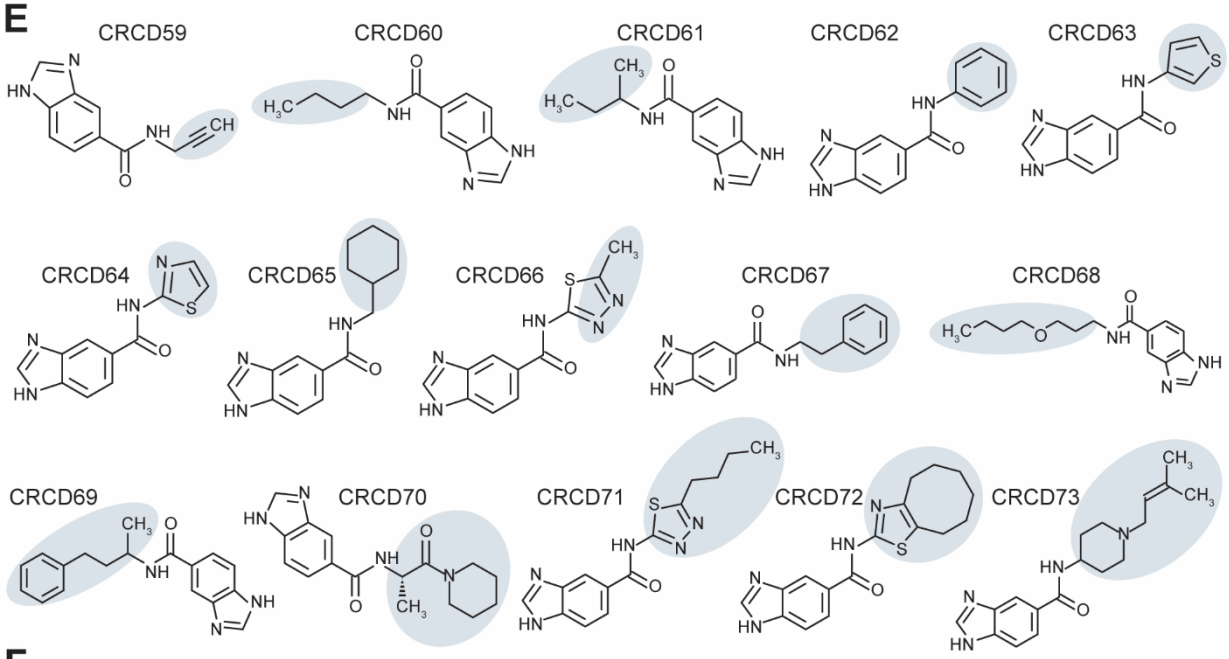

F

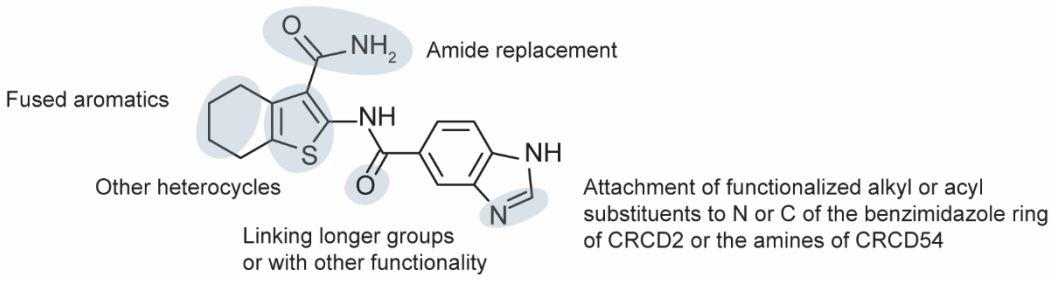

Figure S3. CRCD2 structure activity relationships. (**A**) Structure activity relationship analysis of benzoimidazole group in CRCD2. (**B**) CRCD2 analogs generated with alternative aromatic and heteroaromatic monocyclic and bicyclic groups substitutions. (**C**) Structure activity relationship analysis of tetrahydrobenzothiophene and carboxamide groups in CRCD2. (**D**) CRCD2 analogs generated by removal of the six-membered ring or replacement with one or two methyl groups. (**E**) Analogs generated by replacement of the 4,5,6,7-tetrahydrobenzo[b]thiophene moiety with alkyl, aromatic, and heteroaromatic systems. Modified chemical groups are highlighted in blue. (**F**) Potential strategies and regions of CRCD2 amenable to chemical modification (shadowed) for generation of analogs with potentially improved potency.

Figure S4

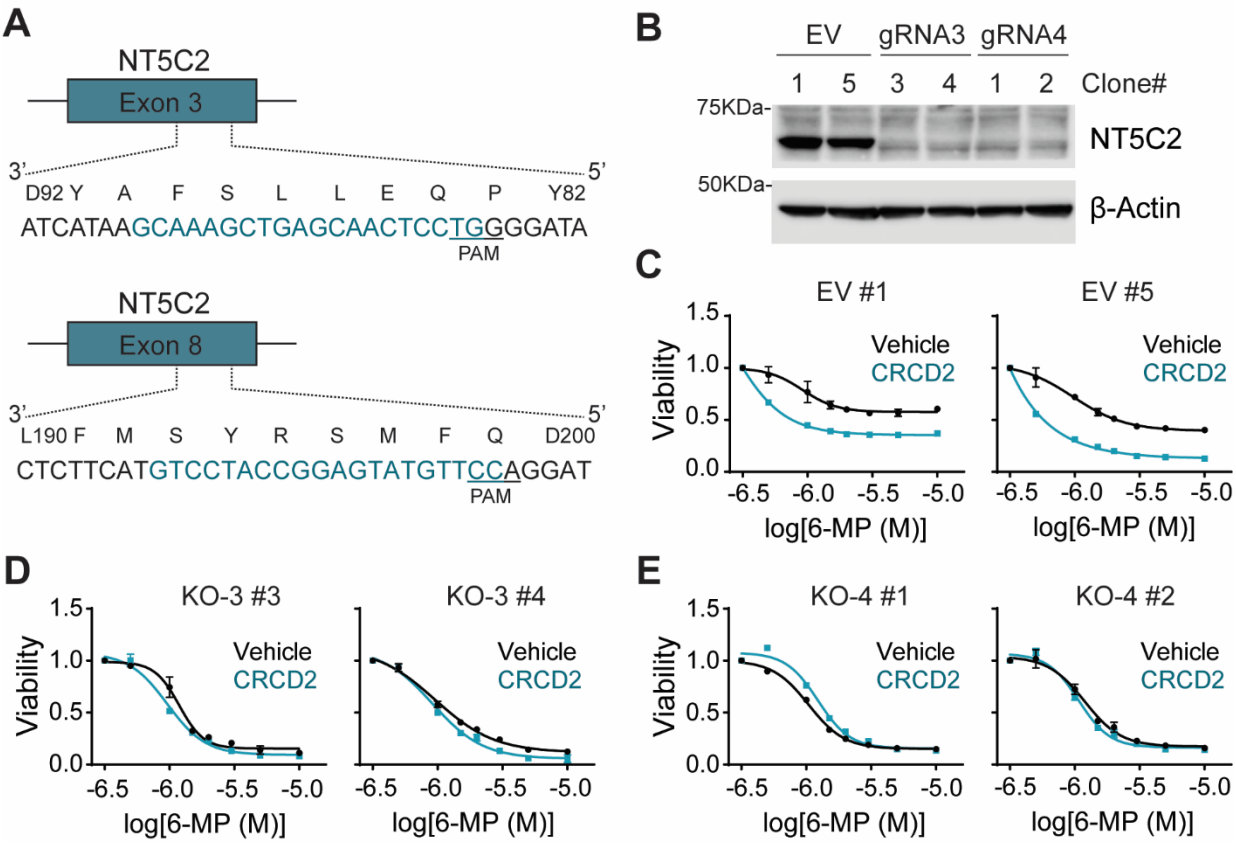

Figure S4. Effect of 6-MP or combination treatment with CRCD2 in human NT5C2 knockout cells. (**A**) Schematic representation of CRISPR NT5C2 knockout strategy. (**B**) Expression of NT5C2 in empty vector or Cas9 + sgRNA transduced CUTLL1 single cell clones. (**C**) Cell viability assays of CUTLL1 single cell clones infected with empty vector treated with vehicle or CRCD2 and increasing doses of 6-MP. (**D**) Cell viability assays of CUTLL1 single cell clones infected with Cas9 + Nt5c2 sgRNA#3 treated as in (**C**). (**E**) Cell viability assays of CUTLL1 single cell clones infected with Cas9 + Nt5c2 sgRNA#4 treated as in (**C**). Graphs show one representative experiment with technical replicates. Two additional experiments showed similar results.

Figure S5

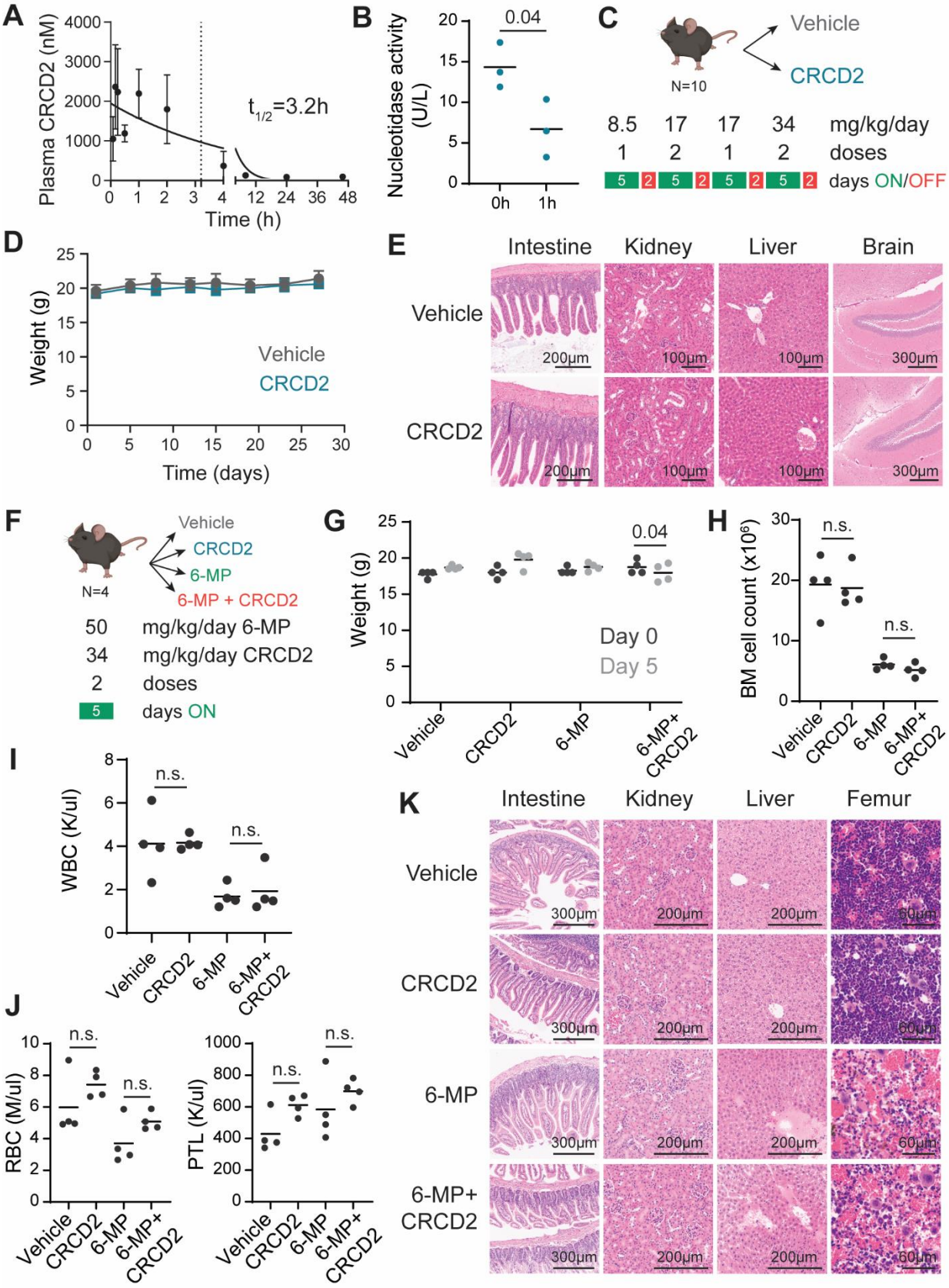
A
Plasma CRCD2 (nM)
4000
3000
2000
1000
0
0 1 2 3 4 12 24 36 48
Time (h)
t1/2=3.2h
B
Nucleotidase activity (U/L)
20
15
10
5
0
0.04
0h
1h
C
N=10
Vehicle
CRCD2
8.5 17 17 34 mg/kg/day
1 2 1 2 doses
5 2 5 2 5 2 5 2 days ON/OFF
D
Weight (g)
25
20
15
10
5
0
0 5 10 15 20 25 30
Time (days)
Vehicle
CRCD2
E
Intestine
Kidney
Liver
Brain
Vehicle
CRCD2
200μm
100μm
100μm
300μm
F
N=4
Vehicle
CRCD2
6-MP
6-MP + CRCD2
50 mg/kg/day 6-MP
34 mg/kg/day CRCD2
2 doses
5 days ON
G
Weight (g)
25
20
15
10
5
0
0.04
Day 0
Day 5
Vehicle
CRCD2
6-MP
6-MP+ CRCD2
H
BM cell count (x10^6)
30
20
10
0
n.s.
n.s.
Vehicle
CRCD2
6-MP
6-MP+ CRCD2
I
WBC (K/ul)
8
6
4
2
0
n.s.
n.s.
Vehicle
CRCD2
6-MP
6-MP+ CRCD2
J
RBC (M/ul)
10
8
6
4
2
0
n.s.
n.s.
PTL (K/ul)
1000
800
600
400
200
0
n.s.
n.s.
Vehicle
CRCD2
6-MP
6-MP+ CRCD2
K
Intestine
Kidney
Liver
Femur
Vehicle
CRCD2
6-MP
6-MP+ CRCD2
300μm
200μm
200μm
60μm

Figure S5. Pharmacokinetics and toxicity analysis of CRCD2 treatment *in vivo*. (**A**) Pharmacokinetics analysis of CRCD2 *in vivo*. Graph shows mean ± SD of three animals treated per time point. Half-life obtained by one phase decay non-linear regression is shown. (**B**) Mouse plasma nucleotidase activity analysis 1h after 17/mg/kg CRCD2 treatment. Graph shows average ± SD of three animals. (**C**) Schematic illustration of tolerance assay using increasing concentrations of CRCD2. (**D**) Mice weight during CRCD2 treatment. Graph shows mean ± SD of five animals treated with vehicle or CRCD2. (**E**) Representative histological micrographs of hematoxylin-eosin stained intestine, kidney, liver and brain tissues from mice treated with vehicle or CRCD2. Analyses of tissues from five mice per group showed similar results. Scale bars are shown. (**F**) Schematic illustration of combination toxicity assay using CRCD2 and 6-MP. (**G**) Mice weight change during toxicity analysis. Graph shows mean ± SD of four animals treated with vehicle, CRCD2, 6-MP or the combination during 5 days. (**H**) Femoral bone marrow cell count after toxicity analysis. Graph shows mean ± SD of four animals treated with vehicle, CRCD2, 6-MP or the combination during 5 days. (**I**) White blood cells analysis after toxicity treatment. Graph shows mean ± SD of 4 animals treated with vehicle, CRCD2, 6-MP or the combination during 5 days. (**J**) Red blood cells and platelets analysis after toxicity treatment. Graph shows mean ± SD of four animals treated with vehicle, CRCD2, 6-MP or the combination during 5 days. (**K**) Representative histological micrographs of hematoxylin-eosin-stained intestine, kidney, liver and femur tissues from mice treated with vehicle, CRCD2, 6-MP or the combination. Analyses of tissues from four mice per group showed similar results. Scale bars are shown. All *P* values were calculated using two-sided Student's t-test.

Figure S6

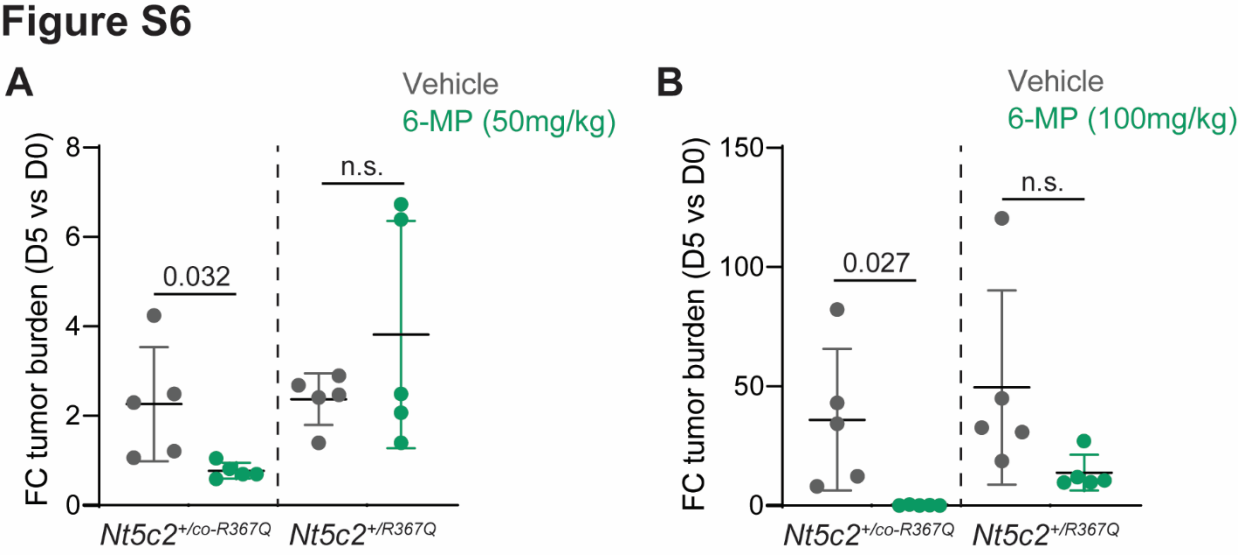

Figure S6. Response of *NT5C2* wild type and R367Q tumors to different doses of 6-MP chemotherapy *in vivo*. (**A**) Luciferase *in vivo* bioimaging analysis of the response of *Nt5c2* wild-type and R367Q mutant ALL tumors treated with 6-MP 50 mg kg^{-1} or vehicle. (**B**) Luciferase *in vivo* bioimaging analysis of the response of *Nt5c2* wild-type and R367Q mutant ALL tumors treated with 6-MP 100 mg kg^{-1} or vehicle. N=5 independent mice per treatment condition. Data are presented as mean values ± SD. *P* values were calculated applying two-sided Student's t-test.

Figure S7

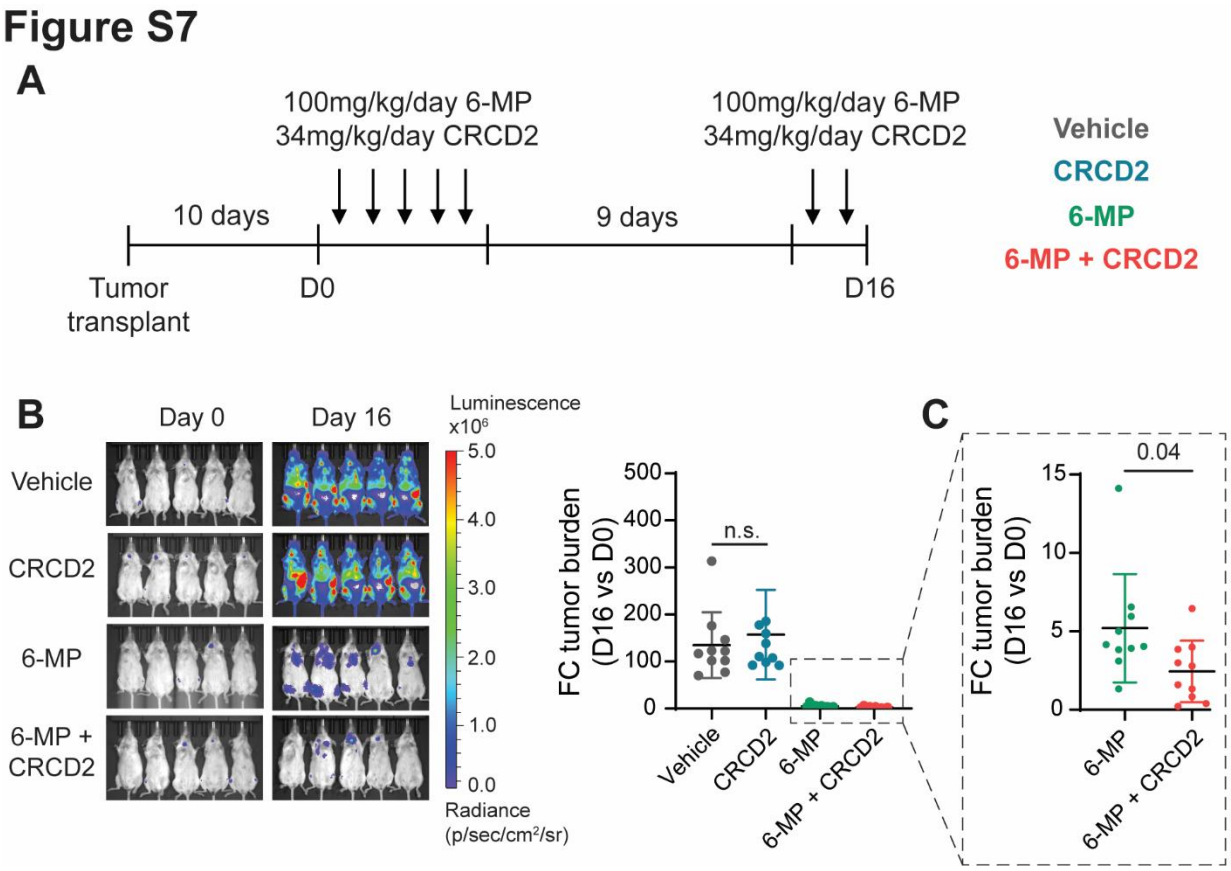

Figure S7. Response of NT5C2 R367Q mutant patient derived xenograft tumors to CRCD2 and 6-MP combinatorial chemotherapy *in vivo*. (**A**) Schematic illustration of 6-MP and CRCD2 combination experimental therapeutic treatment in NT5C2 R367Q mutant T-ALL PDX model. (**B**) Luciferase *in vivo* bioimaging analysis of tumor response (fold change in bioluminescence relative to the basal signal before treatment) in PDX R367Q T-ALL tumors treated with vehicle, single drug or 6-MP and CRCD2 in combination. (**C**) Separate representation of tumor response (fold change in bioluminescence relative to the basal signal before treatment) in PDX R367Q T-ALL tumors treated with 6-MP single-drug or 6-MP and CRCD2 combination also shown in (**B**). N = 10 independent mice per treatment condition. Data are presented as mean values ± SD. *P* values were calculated applying two-sided Student's t-test.

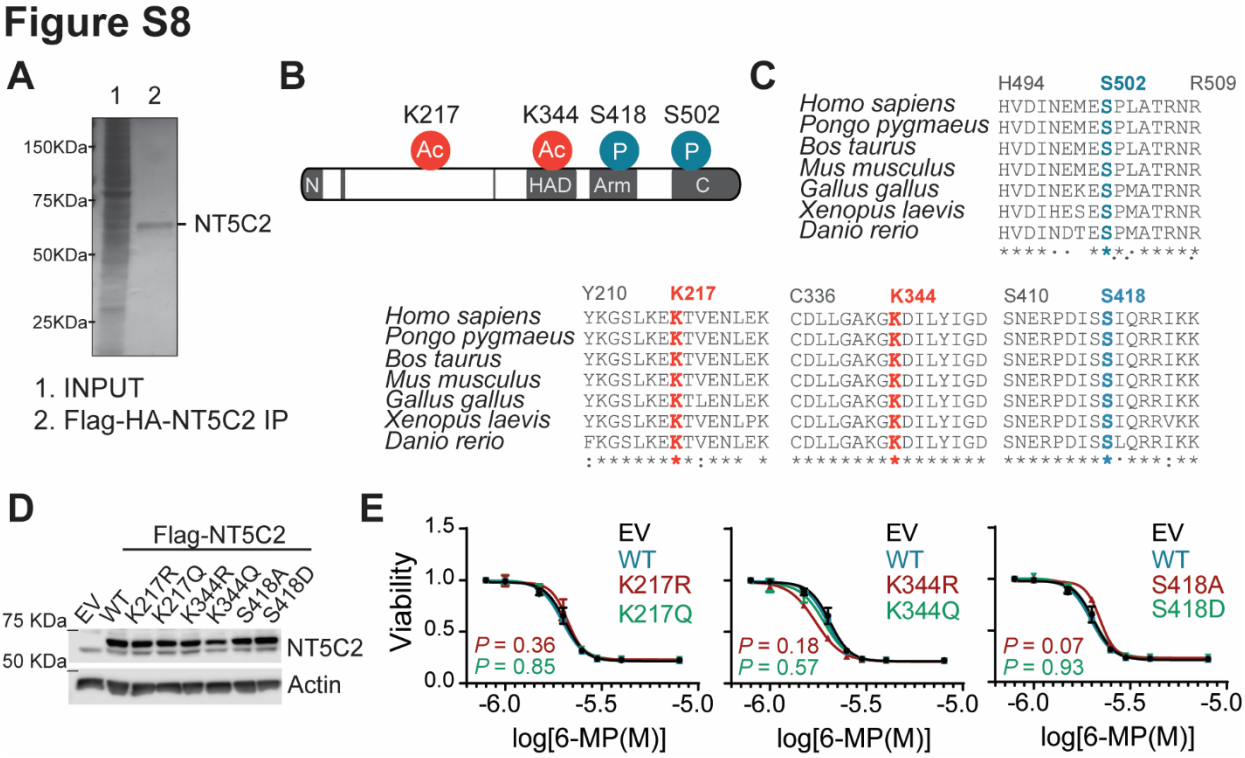

Figure S8. Identification and molecular characterization of NT5C2 post-translational modifications. (**A**) Silver staining showing HA elution from NT5C2 Flag-HA immunoprecipitation from Jurkat cells. (**B**) Schematic illustration of NT5C2 post-translational modifications identified by mass spectrometry analysis. (**C**) Vertebrate species alignment on Lys217, Lys344, Ser418 and Ser502 regions. (**D**) Immunoblot analysis of Jurkat cells infected with empty vector or lentiviruses driving the expression of Flag-tagged Lys217, Lys344 and Ser418 disruptive and mimic mutants of NT5C2. Expression levels were verified in three independent experiments. (**E**) Viability assay of Jurkat cells infected with mutant Lys217, Lys344 and Ser418 NT5C2 expressing lentiviruses treated with increasing doses of 6-MP. Graphs show mean ± SD of three independent experiments performed in triplicate. *P* values were calculated using IC50 values and two-tailed Student's t-test over wild-type.

Figure S9

A

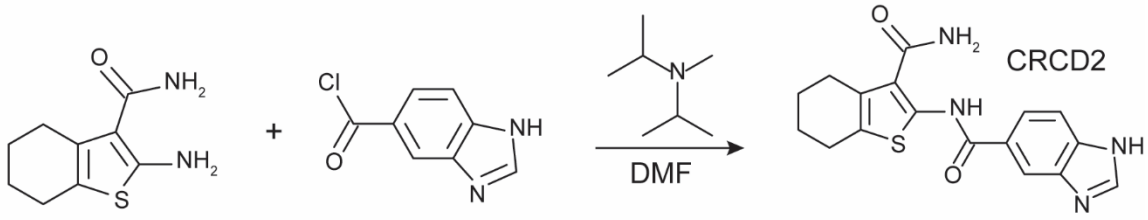

B

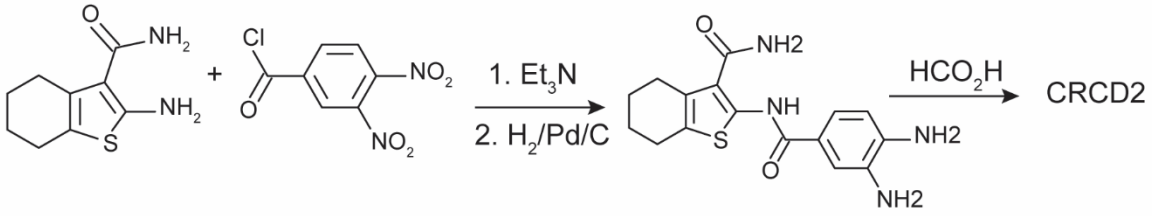

C

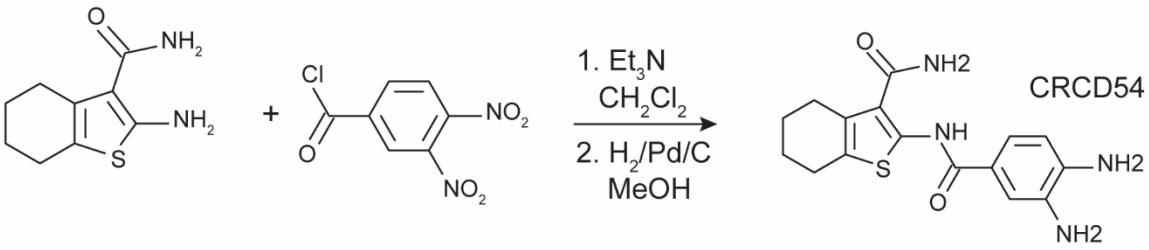

D

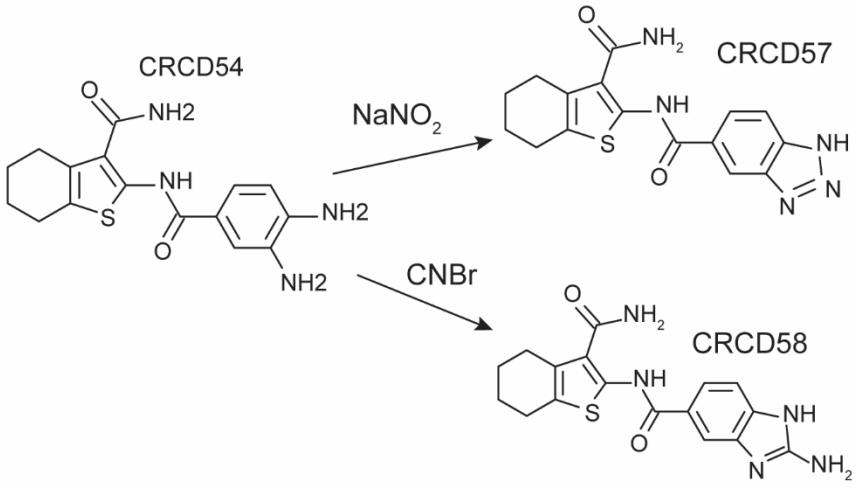

Figure S9. CRCD2 and related analogs syntheses. (**A**) CRCD2 synthesis by treatment of 1H-benzo[d]imidazole-5-carbonyl chloride with 2-amino-4,5,6,7-tetrahydrobenzo[b]thiophene-3-carboxamide and diisopropylethylamine in DMF followed by purification by reverse phase HPLC. (**B**) CRCD2 synthesis by treating the diamine CRCD54 with formic acid. (**C**) CRCD54 synthesis by reaction of 2-amino-4,5,6,7-tetrahydrobenzo[b]thiophene-3-carboxamide with 3,4-dinitrobenzoyl chloride and triethylamine in dichloromethane followed by reduction of the dinitro compound with hydrogen and palladium on carbon in methanol. (**D**) Benzotriazole CRCD57 synthesis by treatment of the diamine CRCD54 with $NaNO_2$ in HOAc, 2-aminobenzoimidazole CRCD8 synthesis by treatment with cyanogen bromide in aqueous methanol.